

Article

Depth Dose Enhancement on Flattening-Filter-Free Photon Beam: A Monte Carlo Study in Nanoparticle-Enhanced Radiotherapy

James C. L. Chow ^{1,2} 

¹ Radiation Medicine Program, Princess Margaret Cancer Centre, University Health Network, Toronto, ON M5G 1X6, Canada; james.chow@rmp.uhn.ca; Tel.: +1-416-946-4501

² Department of Radiation Oncology, University of Toronto, Toronto, ON M5T 1P5, Canada

Received: 24 August 2020; Accepted: 7 October 2020; Published: 11 October 2020



Abstract: The aim of this study is to investigate the variations of depth dose enhancement (DDE) on different nanoparticle (NP) variables, when using the flattening-filter-free (FFF) photon beam in nanoparticle-enhanced radiotherapy. Monte Carlo simulation under a macroscopic approach was used to determine the DDE ratio (DDER) with variables of NP material (gold (Au) and iron (III) oxide (Fe₂O₃)), NP concentration (3–40 mg/mL) and photon beam (10 MV flattening-filter (FF) and 10 MV FFF). It is found that Au NPs had a higher DDER than Fe₂O₃ NPs, when the depths were shallower than 6 and 8 cm for the 10 MV FF and 10 MV FFF photon beams, respectively. However, in a deeper depth range of 10–20 cm, DDER for the Au NPs was lower than Fe₂O₃ NPs mainly due to the beam attenuation and photon energy distribution. It is concluded that DDER for the Au NPs and Fe₂O₃ NPs decreased with an increase of depth in the range of 10–20 cm, with rate of decrease depending on the NP material, NP concentration and the use of FF in the photon beam.

Keywords: nanomaterial; gold nanoparticles; iron oxide nanoparticles; cancer therapy; depth dose enhancement; Monte Carlo simulation; and nanoparticle-enhanced radiotherapy

1. Introduction

In cancer therapy using radiation beams, ionizing particles such as photons are used to damage the DNA of cancer cells, terminate the cell reproduction and hence stop the tumour growth [1,2]. As the external radiation beams have to pass through the patient's skin surface to reach the tumour, irradiation of normal tissues along the path of beam is inevitable. Therefore, the aim of radiotherapy is to give a high dose of radiation to the tumour, while at the same time sparing the surrounding normal tissues and organs. Recently, heavy-atom nanomaterials such as metallic and metal oxide nanoparticles (NPs) are studied as radiosensitizers in radiotherapy [3–6]. The high atomic number of heavy-atom NPs increases the compositional atomic number of the tumour, when the particles are uptaken by the cancer cells. Energy deposition or radiation dose at the cancer cell therefore increases due to the enhancement of photoelectric effect, because of the high atomic number [7,8]. This increase of photon absorption at the tumour relative to its surrounding also causes an imaging contrast enhancement, so that radiation staff can identify the tumour in an imaging modality, such as computed tomography, more accurately [9–11]. NPs not only act as a dose enhancer, but an effective imaging contrast agent in radiotherapy [12]. Although photoelectric effect is recognized as the main mechanism in the dose enhancement, it is found that the radiosensitization enhancement factors for the 35 keV (1.66) and 660 keV (1.18) photon beams are very close to measurements using gold (Au) NPs [13]. This is due to the increased low-energy electron yield and the range of the 660 keV photon beam. This finding opens the door of probability for nanoparticle-enhanced radiotherapy using MV photon beams [14].

For a medical linear accelerator (linac) to deliver a homogeneous dose distribution within the tumour volume, a flattening filter (FF) is required to be installed inside the linac head. The function of the filter is to flatten the photon beam profile produced by the target of the linac [15]. Although the application of FF can improve the dose distribution at the tumour, the filter has disadvantages of increasing the linac head scatter and decreasing of dose rate [16,17]. Since the introduction of intensity modulated radiotherapy, multileaf collimator is employed to generate beam intensity modulation in treatment delivery [18]. As the dose distribution in the tumour can now be controlled by the multileaf collimator, FF can be removed from the linac head to produce a flattening-filter-free (FFF) photon beam. Without the beam attenuation from the FF, the output of the FFF photon beam can be increased from 600 to over 2,000 monitor units per minute [19,20]. In addition, the FFF photon beam also avoids the head scatter from the FF, and shortens the treatment time. Nowadays, FFF photon beam has become a popular option to replace the FF beam in intensity modulated radiotherapy [21–23].

In nanoparticle-enhanced radiotherapy, treatment plan dosimetry between the FF and FFF photon beams is different [24]. It is because the FFF beam contains a greater number of low-energy photons due to the absence of the FF. These low-energy photons are removed by the FF, so beam hardening effect occurs in the FF photon beam [16,17]. The difference in the photon energy spectrum between the FF and FFF beams leads to variations in dose and imaging contrast enhancement [10,19]. This is because both the dose and imaging contrast enhancement depend mainly on the photoelectric effect, which is sensitive to the low-energy photon and the atomic number of the medium [7,8]. It is therefore worthwhile to investigate the dose variation when the FF is removed from the linac in nanoparticle-enhanced radiotherapy.

Monte Carlo simulation is used to determine the radiation dose and calculate the dose enhancement ratio in nanoparticle-enhanced radiotherapy [25,26]. Monte Carlo simulation is a computing algorithm to predict numerical solution of a problem based on random sampling, and is established as a benchmark in dose calculation for radiotherapy [27]. In this study, we assumed the NPs were distributed evenly in the patient, with the radiation beams cross-fired the tumour to conform the dose at the cancer cells. Two types of NPs were used, namely, gold and iron oxide. Au NPs are the most popular nanomaterials used in nanoparticle-enhanced radiotherapy due to their biocompatibility, availability, low cost and high atomic number [28]. Gold nanoparticles have been proved to be an effective radiosensitizer in radiotherapy and computed tomography imaging [29]. On the other hand, magnetic NPs (e.g., Fe₂O₃ NPs) have been proved to be an effective contrast agent in magnetic resonance imaging (MRI) [30,31]. The magnetic property of Fe₂O₃ NPs, which cannot be found in Au NPs, makes the particles applicable in some advanced radiotherapy techniques such as MR guided-radiotherapy using the MRI-linac [32]. The aim of this study is to investigate the variation of depth dose enhancement (DDE) between the FF and FFF photon beams, when Au NPs and Fe₂O₃ NPs are used in radiotherapy.

2. Materials and Methods

2.1. Monte Carlo Phase-Space Files for the FF and FFF Photon Beams

The FF and FFF photon beams used in this study were simulated based on the Varian TrueBeam linac (Varian Medical System, Palo Alto, CA, USA), using the Geant4 [33] and EGSnrc-based BEAMnrc Monte Carlo code [34]. Phase-space files containing information of particles on the scoring plane (e.g., particle type, orientation, position and energy) were generated using beam energy of 10 MV and field size equal to 10 × 10 cm². With the geometric information and configuration of the linac head provided by the vendor, the linac head was modeled using the Geant4 code from the beam source to the phase-space plane just over the jaws. This phase-space plane was then used as a source to generate another plane under the jaws using the BEAMnrc code [35], where we could control the field size produced by the jaws (secondary collimator) conveniently using its component module approach. The phase-space files of the 10 MV FF and FFF photon beams were generated using Monte Carlo simulation, and each file contained 1 × 10⁹ particles. Verification of the Monte Carlo model was carried

out by comparing the Monte Carlo dosimetry with experimental measurements using the scanning water tank and ionization chamber for treatment planning system commissioning. Results of Monte Carlo verification can also be found elsewhere [16,17].

2.2. Depth Doses of the Photon Beams

The depth doses of the 10 MV FF and FFF photon beams were determined by a water phantom with source-to-axis distance equal to 100 cm using the DOSXYZnrc Monte Carlo code [36]. Water was selected as the phantom medium because it is equivalent to the human soft tissue. NP materials of gold and iron (III) oxide were added to the water with concentrations in the range of 3–40 mg/mL. This NP concentration range was used to perform preclinical experiments in nanoparticle-enhanced radiotherapy [25,37]. In this study, we assumed the NPs were distributed evenly in the patient. The material information for simulation was based on the material data library of NPs using the EGSnrc-based PEGS code [34]. In the simulation under the macroscopic approach [26,38], depth doses of the 10 MV FF and FFF photon beams along the central beam axis were determined, with the Au NPs and Fe₂O₃ NPs added to water at different concentrations. All the beam geometry and setting of the Monte Carlo parameters were the same in each simulation, and the number of histories was set to 200 million.

2.3. Calculation of the DDE Ratio (DDER)

The DDER in this study is defined as:

$$\text{Depth Dose Enhancement Ratio (DDER)} = \frac{\text{Depth Dose (d)}_{\text{NPs}}}{\text{Depth Dose (d)}_{\text{Water}}} \quad (1)$$

In Equation (1), Depth Dose (d)_{NPs} is the dose at depth d with NPs added to the medium (water), while Depth Dose (d)_{Water} is the dose at the same depth with no NP added (i.e., water only). It should be noted that the DDER is a function of depth. This is because the energy deposition in the phantom depends on the particle interaction based on the photon energy spectrum, which varies with depth because of the beam attenuation along the central beam axis [16]. When DDER is greater than one, there is a dose enhancement.

3. Results

The DDER vs. depth for different Au NP concentrations using the 10 MV FF and 10 MV FFF photon beams are plotted in Figure 1a,b, while similar results for different Fe₂O₃ NP concentrations are plotted in Figure 2a,b, respectively. To avoid the unstable dose buildup region of the 10 MV photon beams, DDERs are only plotted in the depth range from 4 to 20 cm [17].

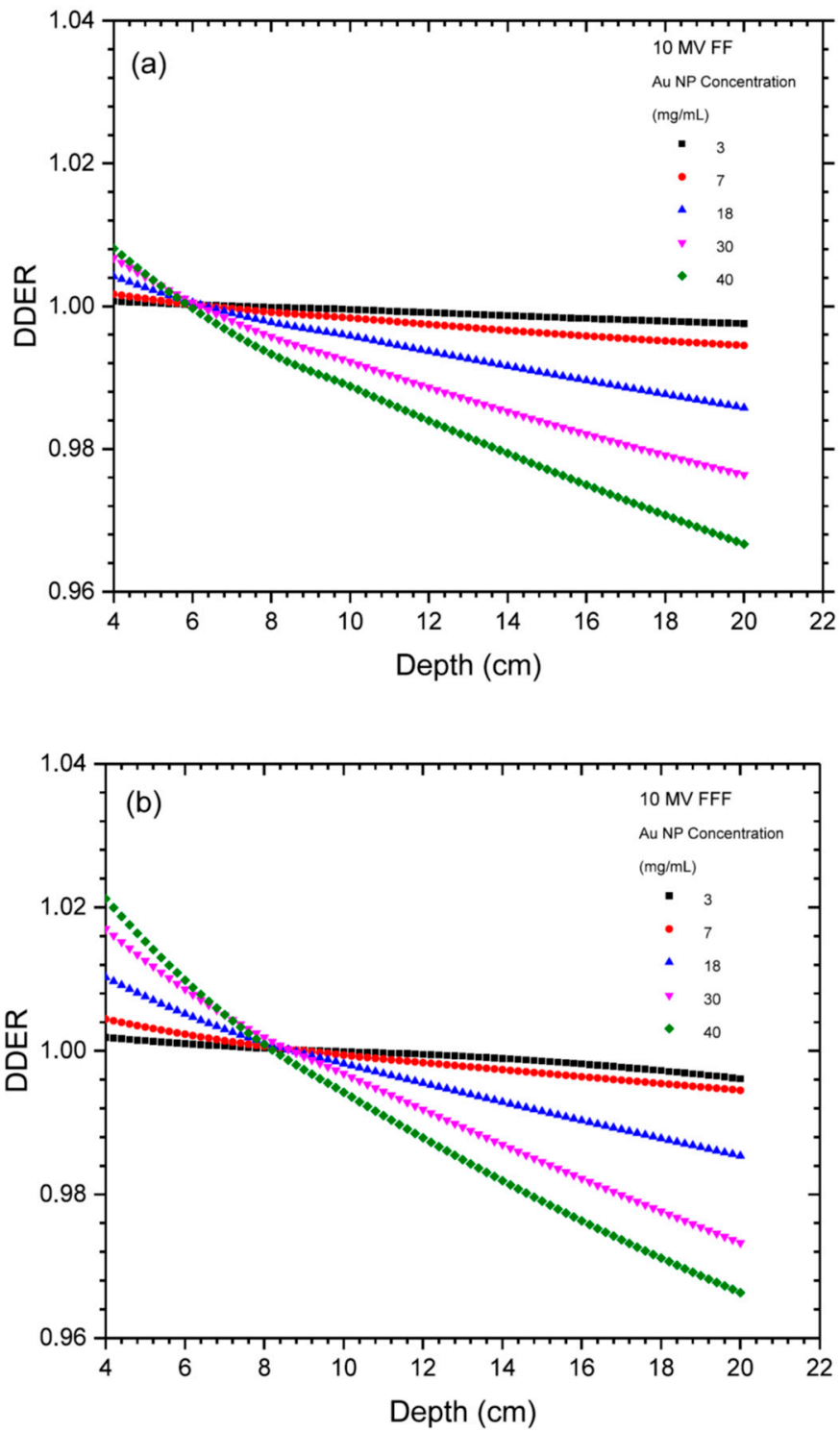


Figure 1. DDER vs. depth for different Au NP concentrations using the (a) 10 MV FF and (b) 10 MV FFF photon beams.

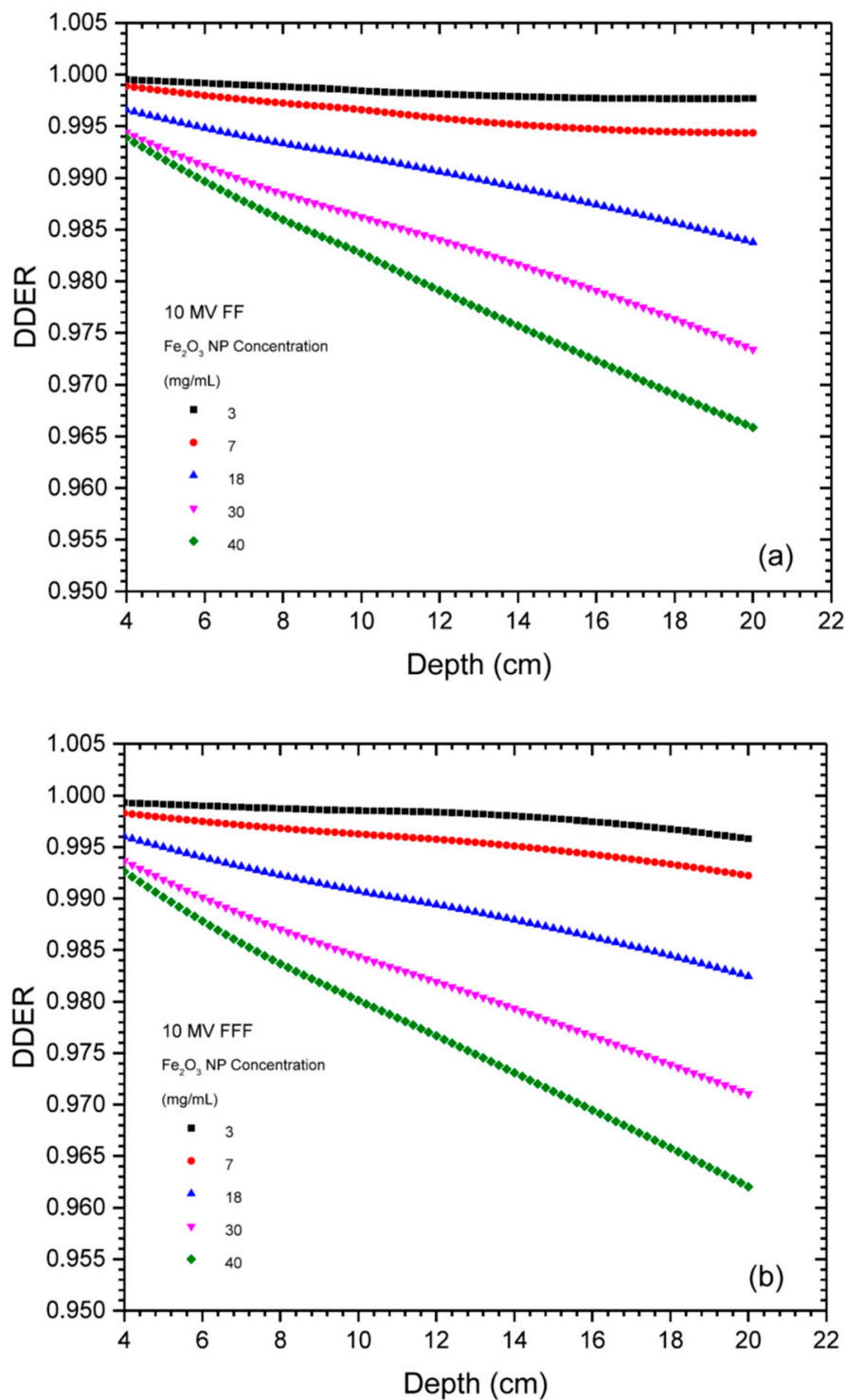


Figure 2. DDER vs. depth for different Fe_2O_3 NP concentrations using the (a) 10 MV FF and (b) 10 MV FFF photon beams.

The DDERs with variations of the NP material and concentration for different depths of phantom are shown in Table 1. Table 1a–d list the DDERs for depths of 5, 10, 15 and 20 cm, respectively.

Table 1. DDERs with variations of the NP material (Au and Fe₂O₃) and concentration for depth equal to (a) 5, (b) 10, (c) 15 and (d) 20 cm using the 10 MV FF and 10 MV FFF photon beams.

(a)	10 MV FF	10 MV FFF	10 MV FF	10 MV FFF
Concentration (mg/mL)	Au NPs	Au NPs	Fe ₂ O ₃ NPs	Fe ₂ O ₃ NPs
3		1.000	1.001	0.999
7		1.001	1.003	0.998
18		1.002	1.008	0.996
30		1.003	1.013	0.993
40		1.004	1.015	0.992
(b)	10 MV FF	10 MV FFF	10 MV FF	10 MV FFF
Concentration (mg/mL)	Au NPs	Au NPs	Fe ₂ O ₃ NPs	Fe ₂ O ₃ NPs
3		1.000	1.000	0.997
7		0.998	0.999	0.997
18		0.996	0.998	0.992
30		0.992	0.997	0.986
40		0.989	0.994	0.983
(c)	10 MV FF	10 MV FFF	10 MV FF	10 MV FFF
Concentration (mg/mL)	Au NPs	Au NPs	Fe ₂ O ₃ NPs	Fe ₂ O ₃ NPs
3		0.998	0.999	0.998
7		0.996	0.997	0.995
18		0.991	0.992	0.988
30		0.984	0.985	0.980
40		0.977	0.979	0.974
(d)	10 MV FF	10 MV FFF	10 MV FF	10 MV FFF
Concentration (mg/mL)	Au NPs	Au NPs	Fe ₂ O ₃ NPs	Fe ₂ O ₃ NPs
3		0.998	0.996	0.998
7		0.995	0.995	0.994
18		0.986	0.985	0.984
30		0.976	0.973	0.973
40		0.967	0.966	0.966

4. Discussion

4.1. Dependence of DDER on Treatment Depth

It can be seen in Figure 1a,b that the DDERs were larger than one, when the depth ranges were 4–6 cm and 4–8 cm, respectively. However, when the depth was more than 6 and 8 cm for the FF and FFF photon beams, the DDERs were less than one, showing that the presence of Au NPs in water could not increase the dose in those depth ranges (i.e., 6–20 cm and 8–20 cm). The addition of Au NPs in water not only enhanced the dose, but also attenuated the photon beam along the depth. When the depth was shallow (i.e., 4–6 and 4–8 cm in Figure 1a,b), the effect of DDE was larger than the beam attenuation. The presence of low-energy photons in the beam at the shallow depth resulted in a dose enhancement [19]. On the other hand, when the depth was deeper and beyond 6 and 8 cm, the effect of beam attenuation became more significant. It is because most of the low-energy photons were absorbed in that depth range, leading to the DDER smaller than one [39]. This shows that the dose in an Au NP-added medium was smaller than the dose in water. In nanoparticle-enhanced radiotherapy, this happens when the NPs cannot be perfectly uptaken by the tumour, leaving particles distributed between the patient surface to the target [40]. This accumulation of NPs in the normal tissues would attenuate the photon beam targeting the tumour, and result in a lower DDE. However, from Table 1, the EEDRs for the FFF photon beams were larger than the FF, for the Au NPs in the depth range

between 5 and 15 cm. Since 5–15 cm is the typical treatment depth in radiotherapy [41], it can be seen that using the FFF photon beams can improve the low DDE due to beam attenuation.

Similar results were observed in Figure 2a,b for the Fe₂O₃ NPs. However, unlike Figure 1a,b, the DDER was all smaller than one in the depth range of 4–20 cm, using the FF and FFF photon beams. The DDE effect for the Fe₂O₃ NPs is therefore lower than the Au NPs.

4.2. Dependence of DDER on the FF and FFF Photon Beams

When the FF is removed from the linac, the FFF beam contains more low-energy photons which would enhance the photoelectric effect and therefore the dose [24]. This can be seen in Table 1a–c for the Au NPs that the DDER for the FFF photon beam was larger than the FF. At a deep depth of 20 cm, the beam attenuation effect was significant as most of the low-energy photons were absorbed in the shallow depth. This caused the DDER of the FFF beam to be smaller than the FF. For the Fe₂O₃ NPs, however, DDER was lower than Au NPs. Therefore, the FFF photon beam was not so effective on the DDE for the Fe₂O₃ NPs compared to Au NPs.

For the depth range of 10–20 cm and NP concentration equal to 18 mg/mL, which is the typical concentration used in preclinical model [37], the DDERs (Figure 1a,b) were found decreased at rates of $1.0 \times 10^{-3} \text{ cm}^{-1}$ and $1.3 \times 10^{-3} \text{ cm}^{-1}$ for the Au NPs, and $0.8 \times 10^{-3} \text{ cm}^{-1}$ and $0.9 \times 10^{-3} \text{ cm}^{-1}$ for the Fe₂O₃ NPs, using the FF and FFF photon beams, respectively. It is found that the DDER of Au NPs decreased at a higher rate than the Fe₂O₃ NPs, and the FFF photon beams decreased at a higher rate than the FF beams. This can be explained by the higher atomic number of gold (79) than iron (26), and the greater number of low-energy photons of the FFF beams than the FF beams [16,24].

4.3. Dependence of DDER on the NP Material and Concentration

In Table 1, it can be seen that Au NPs produced a higher DDER than Fe₂O₃ NPs. However, this also resulted in a higher beam attenuation with depth in the phantom. When NPs are only uptaken by the tumour with NP concentration in the surrounding normal tissues equal to zero, Au NPs are better than Fe₂O₃ NPs in radiotherapy [24,25]. In addition, the use of FFF photon beam also contributes to the DDE when the treatment depth is shallow. Therefore, it is important to develop a NP carrier in order to maximize the NP uptake at the tumour [28,42].

In Figure 1, it can be seen that high concentration of Au NPs had a high DDER but at the same time a high beam attenuation. Similarly, low concentration of Au NPs had a relatively lower DDER but a lower beam attenuation. These characteristics made the DDER curves with different concentrations overlap one another with intersections at about 6 cm (Figure 1a) and 8 cm (Figure 1b). This means that at certain depths, the DDE of the Au NPs would be offset by the beam attenuation due to the variation of the NP concentration.

Considering the Au NP concentration, it is found that the DDERs increased from 1 to 1.004 and 1.001 to 1.015 for concentration range of 3–40 mg/mL, using the FF and FFF photon beams at a depth of 5 cm (Table 1a). However, when the depth was deeper than 5 cm, the DDER was found decreased with an increase of concentration for both the FF and FFF beams. This shows that the beam attenuation was not significant in the shallow depth, which contained more low-energy photons in the beam for an increase of energy deposition. For Fe₂O₃ NPs, the DDER was found decreased with an increase of NP concentration. In this event, the atomic number of iron was not high enough compared to gold to produce a similar DDE in the shallow depth ($d = 5 \text{ cm}$).

When the Au NP concentration was increased from 3 to 40 mg/mL, the DDERs were decreased at rates from 0.2×10^{-3} to $2.2 \times 10^{-3} \text{ cm}^{-1}$ and 0.4×10^{-3} to $2.8 \times 10^{-3} \text{ cm}^{-1}$ for the FF and FFF photon beams, respectively. For Fe₂O₃ NPs, relatively lower rates of $0.1\text{--}1.7 \times 10^{-3} \text{ cm}^{-1}$ and $0.3\text{--}1.8 \times 10^{-3} \text{ cm}^{-1}$ were found for the FF and FFF beams. Therefore, it is seen that increasing the NP concentration increased the rate of decreased dose enhancement with depth (Figures 1 and 2), and such effect was more significant in Au NPs.

5. Conclusions

Dependences of DDER on variables such as NP concentration, NP material and the use of the FF in the photon beam were investigated using Monte Carlo simulation under a macroscopic approach. It is concluded that the DDER decreased with depth in the range of 6–20 cm (FF photon beam) and 8–20 cm (FFF photon beam) for the Au NPs, and 4–20 cm (FF and FFF photon beams) for the Fe₂O₃ NPs. For the depth along the central beam axis, Au NPs had a higher beam attenuation than Fe₂O₃ NPs. Moreover, for both the Au NPs and Fe₂O₃ NPs, DDERs were found decreased at a higher rate when the NP concentration increased. Future work includes studying the dependence of DDER on the photon beam energy. Results in this study are useful for radiation staff when considering what NP material and NP concentration should be used in nanoparticle-enhanced radiotherapy delivered by the FFF photon beams.

Funding: This research received no external funding.

Acknowledgments: The author would like to thank Amir Owrangi in UT Southwestern Medical Centre for assistance in the phase-space files and photon energy spectra of the FFF and FF photon beams used in the Monte Carlo simulations. The author would also like to thank Joyal Thomas in Ryerson University for his assistance in the Monte Carlo simulations in the beginning of this work.

Conflicts of Interest: The author declares no conflict of interest.

References

1. Lomax, M.E.; Folkes, L.K.; O’neill, P. Biological consequences of radiation-induced DNA damage: Relevance to radiotherapy. *Clin. Oncol.* **2013**, *25*, 578–585. [[CrossRef](#)] [[PubMed](#)]
2. Chun, H.; Chow, J.C.L. Gold nanoparticle DNA damage in radiotherapy: A Monte Carlo study. *AIMS Bioeng.* **2016**, *3*, 352–361.
3. Chow, J.C.L. Recent Progress of Gold Nanomaterials in Cancer Therapy. In *Handbook of Nanomaterials and Nanocomposites for Energy and Environmental Applications*; Kharissova, O.V., Torres-Martínez, L.M., Kharisov, B.I., Eds.; Springer Nature: Cham, Switzerland, 2020; pp. 1–30.
4. Chow, J.C.L. Application of Nanoparticle Materials in Radiation Therapy. In *Handbook of Ecomaterials*; Martínez, L.M.T., Kharissova, O.V., Kharisov, B.I., Eds.; Springer Nature: Cham, Switzerland, 2017; Chapter 150; pp. 3661–3681.
5. Rosa, S.; Connolly, C.; Schettino, G.; Butterworth, K.T.; Prise, K.M. Biological mechanisms of gold nanoparticle radiosensitization. *Cancer Nanotechnol.* **2017**, *8*, 2. [[CrossRef](#)] [[PubMed](#)]
6. Butterworth, K.T.; McMahan, S.J.; Currell, F.J.; Prise, K.M. Physical basis and biological mechanisms of gold nanoparticle radiosensitization. *Nanoscale* **2012**, *4*, 4830–4838. [[CrossRef](#)] [[PubMed](#)]
7. Chow, J.C.L. Characteristics of secondary electrons from irradiated gold nanoparticle in radiotherapy. In *Handbook of Nanoparticles*; Aliofkhaezrai, M., Ed.; Springer International Publishing: Cham, Switzerland, 2015; Chapter 10; pp. 1–18.
8. Chow, J.C.L. Photon and electron interactions with gold nanoparticles: A Monte Carlo study on gold nanoparticle-enhanced radiotherapy. In *Nanobiomaterials in Medical Imaging: Applications of Nanobiomaterials*; Grumezescu, A.M., Ed.; Elsevier: Amsterdam, The Netherlands, 2016; Chapter 2; pp. 45–70.
9. Mututantri-Bastiyange, D.; Chow, J.C.L. Imaging dose of cone-beam computed tomography in nanoparticle-enhanced image-guided radiotherapy: A Monte Carlo phantom study. *AIMS Bioeng.* **2020**, *7*, 1–11. [[CrossRef](#)]
10. Abdulle, A.; Chow, J.C.L. Contrast enhancement for portal imaging in nanoparticle-enhanced radiotherapy: A Monte Carlo phantom evaluation using flattening-filter-free photon beams. *Nanomaterials* **2019**, *9*, 920. [[CrossRef](#)]
11. Albayedh, F.; Chow, J.C.L. Monte Carlo simulation on the imaging contrast enhancement in nanoparticle-enhanced radiotherapy. *J. Med. Phys.* **2018**, *43*, 195–199.
12. Chow, J.C.L. Dose Enhancement Effect in Radiotherapy: Adding Gold Nanoparticle to Tumour in Cancer Treatment. In *Nanostructures for Cancer Therapy*; Ficaí, A., Grumezescu, A.M., Eds.; Elsevier: Amsterdam, The Netherlands, 2017; Chapter 15; pp. 383–400.

13. Chithrani, D.B.; Jelveh, S.; Jalali, F.; van Prooijen, M.; Allen, C.; Bristow, R.G.; Hill, R.P.; Jaffray, D.A. Gold nanoparticles as radiation sensitizers in cancer therapy. *Rad. Res.* **2010**, *173*, 719. [[CrossRef](#)]
14. Chow, J.C.L.; Leung, M.K.K.; Fahey, S.; Chithrani, D.B.; Jaffray, D.A. Monte Carlo simulation on low-energy electrons from gold nanoparticle in radiotherapy. *J. Phys. Conf. Ser.* **2012**, *341*, 012012. [[CrossRef](#)]
15. Lutz, W.R.; Larsen, R.D. The effect of flattening filter design on quality variations within an 8-MV primary x-ray beam. *Med. Phys.* **1984**, *11*, 843–845. [[CrossRef](#)]
16. Chow, J.C.L.; Owrangi, A.M. A surface energy spectral study on the bone heterogeneity and beam obliquity using the flattened and unflattened photon beams. *Rep. Pract. Oncol. Radiother.* **2016**, *21*, 63–70. [[CrossRef](#)] [[PubMed](#)]
17. Chow, J.C.L.; Owrangi, A.M. Dosimetric dependences of bone heterogeneity and beam angle on the unflattened and flattened photon beams: A Monte Carlo comparison. *Rad. Phys. Chem.* **2014**, *101*, 46–52. [[CrossRef](#)]
18. Bortfeld, T. IMRT: A review and preview. *Phys. Med. Biol.* **2006**, *51*, R363. [[CrossRef](#)] [[PubMed](#)]
19. Chow, J.C.L.; Owrangi, A.M. Mucosal dosimetry on unflattened photon beams: A Monte Carlo phantom study. *Biomed. Phys. Eng. Express* **2019**, *5*, 015007. [[CrossRef](#)]
20. Vassiliev, O.N.; Titt, U.; Pönisch, F.; Kry, S.F.; Mohan, R.; Gillin, M.T. Dosimetric properties of photon beams from a flattening filter free clinical accelerator. *Phys. Med. Biol.* **2006**, *51*, 1907. [[CrossRef](#)] [[PubMed](#)]
21. Nicolini, G.; Ghosh-Laskar, S.; Shrivastava, S.K.; Banerjee, S.; Chaudhary, S.; Agarwal, J.P.; Munshi, A.; Clivio, A.; Fogliata, A.; Mancosu, P.; et al. Volumetric modulation arc radiotherapy with flattening filter-free beams compared with static gantry IMRT and 3D conformal radiotherapy for advanced esophageal cancer: A feasibility study. *Int. J. Radiat. Oncol. Biol. Phys.* **2012**, *84*, 553–560. [[CrossRef](#)] [[PubMed](#)]
22. Arslan, A.; Sengul, B. Comparison of radiotherapy techniques with flattening filter and flattening filter-free in lung radiotherapy according to the treatment volume size. *Sci. Rep.* **2020**, *10*, 1–8. [[CrossRef](#)]
23. Sharma, M.; Chow, J.C.L. Skin dose enhancement from the application of skin-care creams using FF and FFF photon beams in radiotherapy: A Monte Carlo phantom evaluation. *AIMS Bioeng.* **2020**, *7*, 82–90. [[CrossRef](#)]
24. Martelli, S.; Chow, J.C.L. Dose enhancement for the flattening-filter-free and flattening-filter photon beams in nanoparticle-enhanced radiotherapy: A Monte Carlo phantom study. *Nanomaterials* **2020**, *10*, 637. [[CrossRef](#)]
25. Zheng, X.J.; Chow, J.C.L. Radiation dose enhancement in skin therapy with nanoparticle addition: A Monte Carlo study on kilovoltage photon and megavoltage electron beams. *World J. Radiol.* **2017**, *9*, 63–71. [[CrossRef](#)]
26. Chow, J.C.L. Recent progress in Monte Carlo simulation on gold nanoparticle radiosensitization. *AIMS Biophys.* **2018**, *5*, 231–244. [[CrossRef](#)]
27. Rogers, D.W. Fifty years of Monte Carlo simulations for medical physics. *Phys. Med. Biol.* **2006**, *51*, R287. [[CrossRef](#)] [[PubMed](#)]
28. Siddique, S.; Chow, J.C.L. Gold nanoparticles for drug delivery and cancer therapy. *Appl. Sci.* **2020**, *10*, 3824. [[CrossRef](#)]
29. Haume, K.; Rosa, S.; Grellet, S.; Śmiałek, M.A.; Butterworth, K.T.; Solov'yov, A.V.; Prise, K.M.; Golding, J.; Mason, N.J. Gold nanoparticles for cancer radiotherapy: A review. *Cancer Nanotechnol.* **2016**, *7*, 8. [[CrossRef](#)] [[PubMed](#)]
30. Kostevšek, N. A Review on the Optimal Design of Magnetic Nanoparticle-Based T2 MRI Contrast Agents. *Magnetochemistry* **2020**, *6*, 11. [[CrossRef](#)]
31. Hu, H. Recent Advances of Bioresponsive Nano-Sized Contrast Agents for Ultra-High-Field Magnetic Resonance Imaging. *Front. Chem.* **2020**, *8*, 203. [[CrossRef](#)] [[PubMed](#)]
32. Chin, S.; Eccles, C.L.; McWilliam, A.; Chuter, R.; Walker, E.; Whitehurst, P.; Berresford, J.; Van Herk, M.; Hoskin, P.J.; Choudhury, A. Magnetic resonance-guided radiation therapy: A review. *J. Med. Imag. Radiat. Oncol.* **2020**, *64*, 163–177. [[CrossRef](#)]
33. Agostinelli, S.; Allison, J.; Amako, K.A.; Apostolakis, J.; Araujo, H.; Arce, P.; Asai, M.; Axen, D.; Banerjee, S.; Barrand, G.; et al. GEANT4—A simulation toolkit. *Nucl. Instrum. Methods Phys. Res. Sect. A Accel. Spectrometers Detect. Assoc. Equip.* **2003**, *506*, 250–303. [[CrossRef](#)]
34. Rogers, D.W.; Kawrakow, I.; Seuntjens, J.P.; Walters, B.R.; Mainegra-Hing, E. NRC user codes for EGSnrc. *NRC Rep. PIRS (Rev. B)* **2003**, 702.
35. Rogers, D.W.; Walters, B.; Kawrakow, I. BEAMnrc users manual. *NRC Rep. PIRS* **2009**, 509, 12.
36. Walters, B.R.; Kawrakow, I.; Rogers, D.W. DOSXYZnrc users manual. *NRC Rep. PIRS* **2005**, 794, 1–25.

37. Hainfeld, J.F.; Slatkin, D.N.; Smilowitz, H.M. The use of gold nanoparticles to enhance radiotherapy in mice. *Phys. Med. Biol.* **2004**, *49*, N309. [[CrossRef](#)] [[PubMed](#)]
38. Chow, J.C.L. Monte Carlo Nanodosimetry in Gold Nanoparticle-Enhanced Radiotherapy. In *Recent Advancements and Applications in Dosimetry*; Chan, M.F., Ed.; Nova Science Publishers: New York, NY, USA, 2018; Chapter 2.
39. Bloch, P.; McDonough, J. Extraction of the photon spectra from measured beam parameters. *Med. Phys.* **1998**, *25*, 752–757. [[CrossRef](#)] [[PubMed](#)]
40. Elsaesser, A.; Taylor, A.; de Yanés, G.S.; McKerr, G.; Kim, E.M.; O'Hare, E.; Howard, C.V. Quantification of nanoparticle uptake by cells using microscopical and analytical techniques. *Nanomedicine* **2010**, *5*, 1447–1457. [[CrossRef](#)] [[PubMed](#)]
41. Barrett, A.; Morris, S.; Dobbs, J.; Roques, T. *Practical Radiotherapy Planning*; CRC Press: Boca Raton, FL, USA, 2009.
42. Siddique, S.; Chow, J.C.L. Application of Nanomaterials in Biomedical Imaging and Cancer Therapy. *Nanomaterials* **2020**, *10*, 1700. [[CrossRef](#)]



© 2020 by the author. Licensee MDPI, Basel, Switzerland. This article is an open access article distributed under the terms and conditions of the Creative Commons Attribution (CC BY) license (<http://creativecommons.org/licenses/by/4.0/>).